Cell Reports, Volume *23*

Supplemental Information

Whole-Cell Scale Dynamic Organization of Lysosomes Revealed by Spatial Statistical Analysis

Qinle Ba, Guruprasad Raghavan, Kirill Kiselyov, and Ge Yang

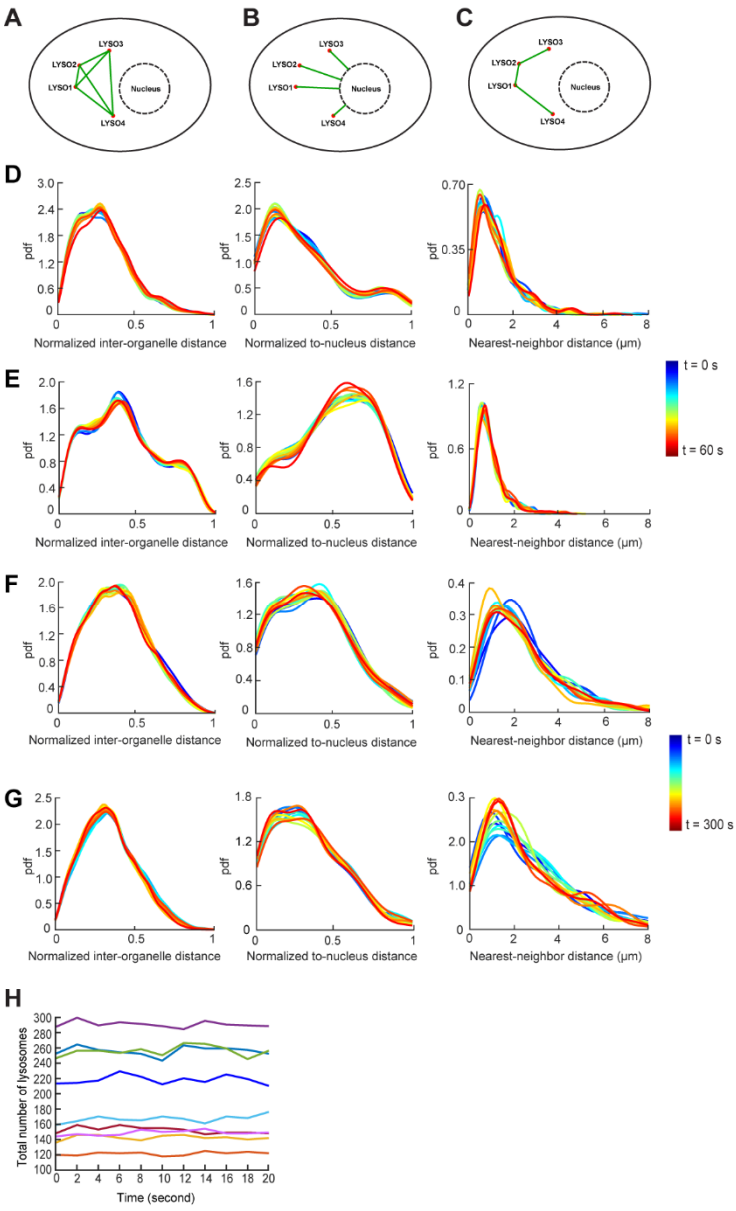

Figure S1. Related to Figure 1. Spatial distributions and total numbers of lysosomes remain stable over time in single cells. (A) A cartoon illustration of inter-organelle distances. (B) A cartoon illustration of to-nucleus distances. (C) A cartoon illustration of nearest-neighbor distances. (D) and (E): Distributions of the three distances of lysosomes from two BS-C-1 cells. Each distribution was plotted every 5 seconds over 60 seconds, hence 13 plots. The temporal variations were quantified using Sorensen dissimilarity scores. A total of 13 distributions were compared pairwise, hence $C_{13}^{2} = 78$ pairs. pdf: probability density function. (D) Temporal variations (mean ± STD; n = 78): normalized inter-organelle distance distribution, 1.77% ± 0.64%; normalized to-nucleus distance distribution, 2.53% ± 0.72%; nearest-neighbor distance distribution, 8.64% ± 2.65%. (E) Temporal variations (mean ± STD; n = 78): normalized inter-organelle distance distribution, 1.87% ± 0.61%; normalized to-nucleus distance distribution: 2.60% ± 1.04%; nearest-neighbor distance distribution, 6.07% ± 1.51%. (F) and (G): three distance distributions of lysosomes from two COS-7 cells. Each distribution was plotted every 25 seconds over 300 seconds, hence 13 plots. (F) Temporal variations (mean ± STD; n = 78): normalized inter-organelle distance distribution, 1.53% ± 1.43%; normalized to-nucleus distance distribution, 2.04% ± 1.75%; nearest-neighbor distance distribution, 5.19% ± 4.47%. (G) Temporal variations (mean ± STD; n = 78): normalized inter-organelle distance distribution, 1.71% ± 1.66%; normalized to-nucleus distance distribution, 1.94% ± 1.63%; nearest-neighbor distance distribution, 5.55% ± 4.49%. (H) Total numbers of lysosomes in COS-7 cells during 20 seconds of imaging, plotted every 2 seconds for each cell, n = 9 cells. Frame rate: 10 frames per second. Total numbers of lysosomes in each cell (mean ± STD): 122 ± 2, 142 ± 3, 149 ± 3, 152 ± 4, 167 ± 5, 218 ± 6, 255 ± 7, 256 ± 6, 290 ± 4.

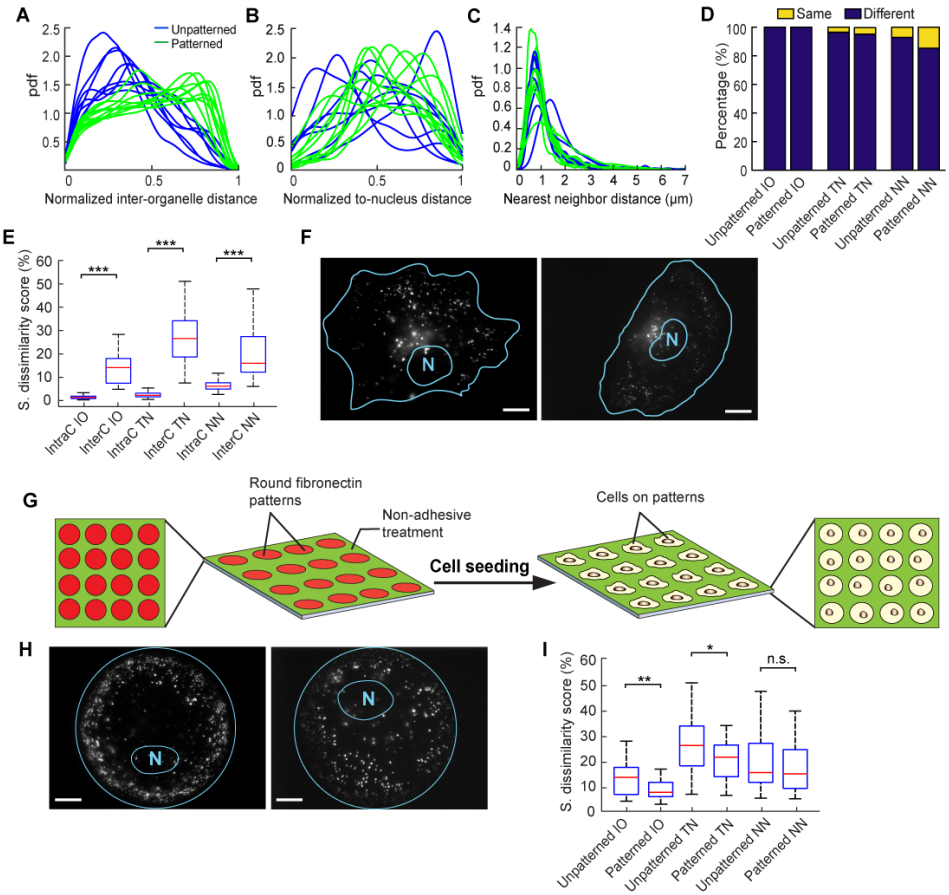

Figure S2. Related to Figure 1. Distinct lysosomal distributions in singles cells are not merely a secondary effect of their distinct shapes. (A-C) Comparison of three distance distributions in non-patterned cells (blue lines; n = 8) and patterned cells (green lines; n = 10). (D) Results of pairwise comparison of the three distance distributions among non-patterned (total = 28 comparisons; left columns) and patterned cells (total = 45 comparisons; right columns) using two-sample Kolmogorov-Smirnov tests. Cutoff p-value for statistical significance: 0.05. IO: normalized inter-organelle distance distribution; TN: normalized to-nucleus distance distribution; NN: nearest-neighbor distance distribution. Percentage of comparison showing significant differences: IO: 100% (non-patterned) and 100% (patterned); TN: 96.4% (non-patterned) and 95.6% (patterned); NN: 92.9% (non-patterned) and 84.4% (patterned). (E) Comparison of intracellular (intraC) variations of the distance distributions within single cells versus intercellular (interC) variations of the distributions among different cells using Wilcoxon rank sum tests. All variations represented in Sorensen dissimilarity scores. IO: intracellular: 1.64% ± 1.38% (mean ± STD; n = 624 scores; data pooled from 8 cells with 78 scores per cell), intercellular: 14.42% ± 7.27% (mean ± STD; n = 28 scores from 8 cells), p-value: 1.3×10^{-18}; TN: intracellular: 2.67% ± 1.80%, intercellular: 27.89% ± 12.83%, p-value: 4.5×10^{-19}; NN: intracellular: 6.46% ± 2.14%, intercellular: 21.53% ± 13.42%, p-value: 1.2×10^{-15}. Notation for p values: *, $p < 0.05$; **, $p < 0.01$; ***, $p < 0.001$. (F) Examples of unpatterned cells with different shapes. Scale bars: 10 μm. (G) A cartoon illustrating the process of patterning shapes of cells by growing them on patterned fibronectin substrates. (H) Examples of patterned cells. Scale bars: 10 μm. (I) Comparison of intercellular variations of non-patterned cells versus patterned cells using one-tailed Wilcoxon rank sum tests. IO: non-patterned: 14.42% ± 7.27% (mean ± STD; n = 28 scores from 8 cells); patterned: 9.42% ± 3.99% (mean ± STD; n = 45 scores from 10 cells), p-value: 0.0037. TN: non-patterned: 27.89% ± 12.83%; patterned: 20.65% ± 7.63%, p-value: 0.016. NN: non-patterned: 21.53% ± 13.42%; patterned: 18.94% ± 10.50%, p-value: 0.59.

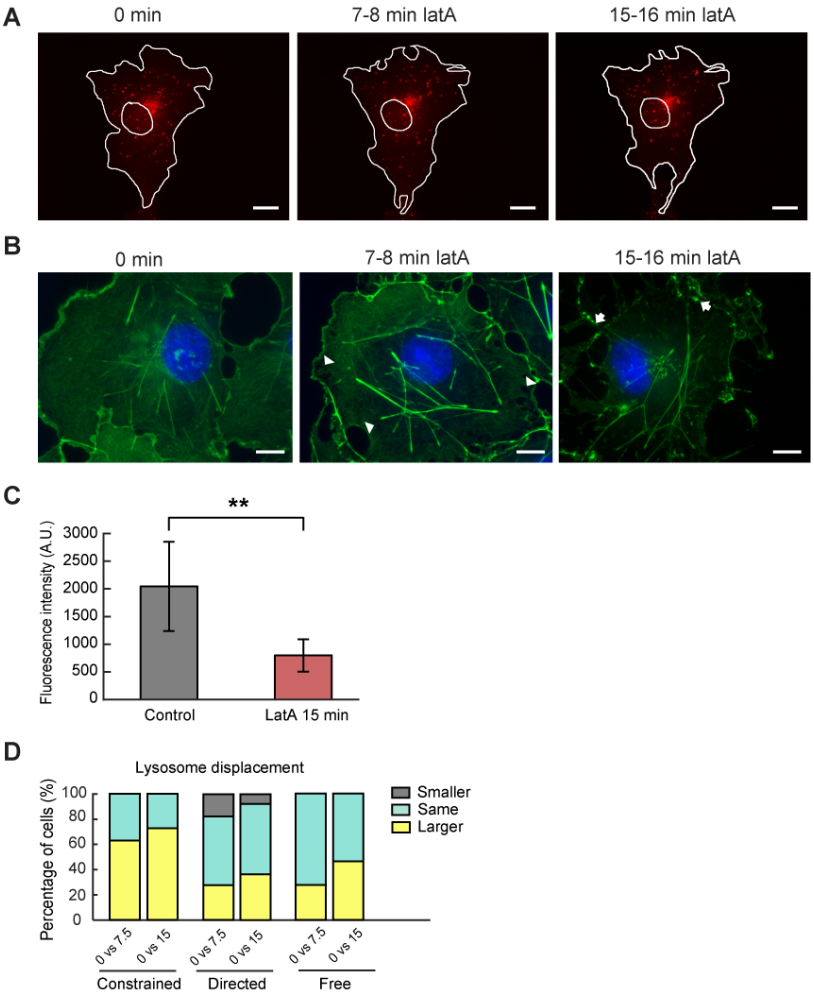

Figure S3. Related to Figure 3. Changes of actin network and lysosomal movement under latrunculin A treatment. (A) Shape changes of a COS-7 cell transfected with mCherry-Lamp1 at different time points before and after treatment of 0.8 μM of latrunculin A. Red, lysosomes. Scale bars: 15 μm. (B) COS-7 cells fixed and stained with phalloidin (Actin-stain 488) under control condition and after 7.5 min and 15 min of latA (0.8 μM) treatment. Arrow heads point to regions with reduced phalloidin fluorescence signals. Arrows point to actin patches. Scale bars, 10 μm. (C) Quantification of fluorescence intensity of actin in control and latA treated cells. A.U., arbitrary unit. Control: 2048 ± 807 (mean ± STD; n = 7 cells); latA 15 min: 799 ± 289 (mean ± STD; n = 7 cells). A one-tailed unpaired student-t test was performed; p-value, 0.0098. (D) Comparison of displacement of different lysosomal subpopulations within 5 seconds before and after latA treatment in single cells: before treatment (0 min) vs 7.5 min; before treatment (0 min) vs. 15 min. n = 11 cells. One-tailed unpaired student-t tests were performed with a cutoff significance level of 0.05. Constrained diffusion, 0 min vs 7.5 min: smaller, 0%; same 36.4%; larger: 63.6%; constrained, 0 min vs 15 min: smaller 0%; same 27.3%; larger 72.7%. Directed movement, 0 vs 7.5 min: smaller 18.2%; same 54.5%; larger 27.3%; directed, 0 vs 15 min: smaller 9.1%; same 54.5%; larger 36.4%. Free diffusion, 0 vs 7.5 min: smaller 0%; same 72.7%; larger 27.3%; free diffusion, 0 vs 15 min: smaller 0%; same 54.5%; larger 45.5%.

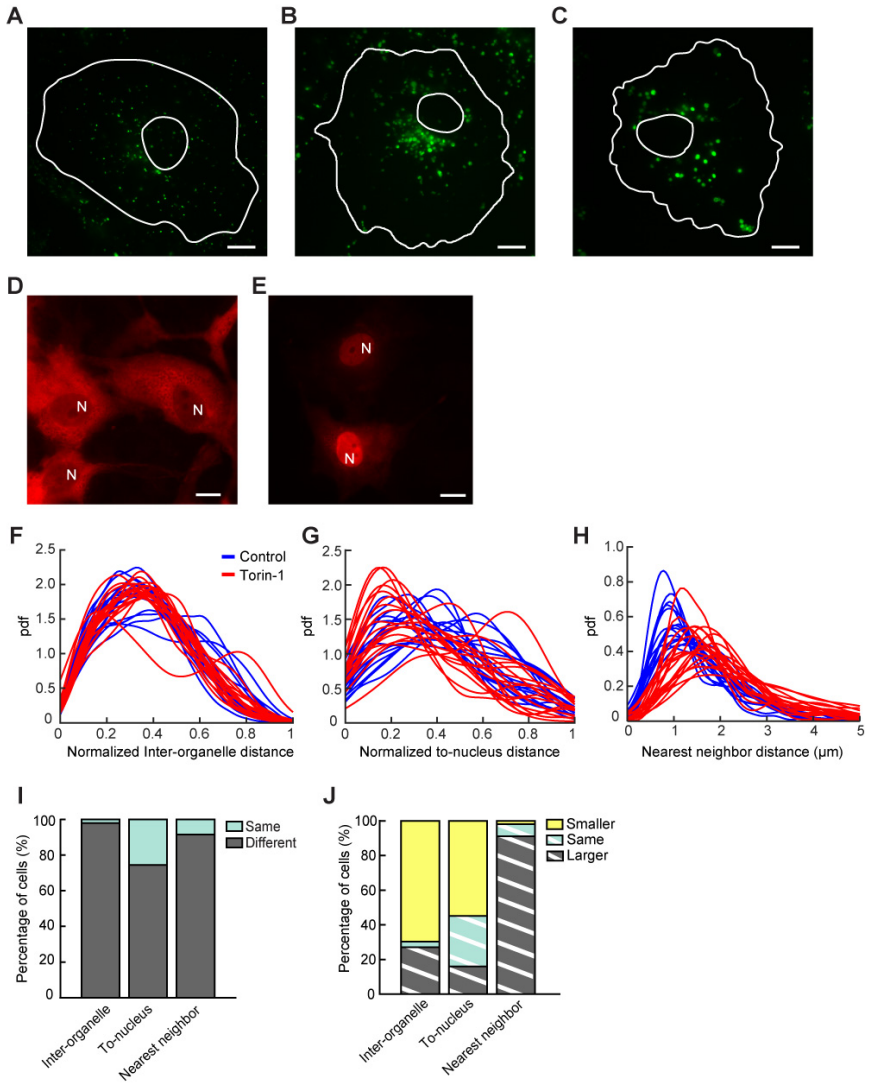

Figure S4. Related to Figure 3. Changes of lysosomal spatial distribution upon torin-1 treatment. (A-C) Changed distributions of lysosomes labeled with dextran Alexa-488 (green) in COS-7 cells under torin-1 treatment. A: Control (DMSO). (B) and (C): Two different cells treated with 2 μM torin-1 for 13.5 hours. Scale bars: 10 μm. (D-E) COS-7 cells transfected with TFEB-myc was stained with rabbit anti-myc antibody and mouse anti-rabbit Alexa 594 secondary antibody. (D) Control (DMSO). N, cell nucleus. (E) 2 μM torin-1 treated for 4 hours. (F-H) The three distance distributions in control cells (n = 15) versus torin-1 treated cells (13.5 hours, 18 cells). (I) Comparison of distributions in control cells versus cells treated with torin-1 using two sample Kolmogorov-Smirnov tests (n = 270 pairs). Inter-organelle (different, same): 99.3%, 0.7%; To-nucleus: 75.7%, 24.3%; Nearest-neighbor: 91.5%, 8.5%. (J) Comparison of median distances in control cells versus cells treated with torin-1 using one-tailed Wilcoxon rank sum tests (n = 270 pairs). Inter-organelle (smaller, same, larger): 69.6%, 3.4%, 27.0%; To-nucleus: 54.8%, 29.2%, 15.9%; Nearest-neighbor: 0.4%, 8.5%, 91.1%.

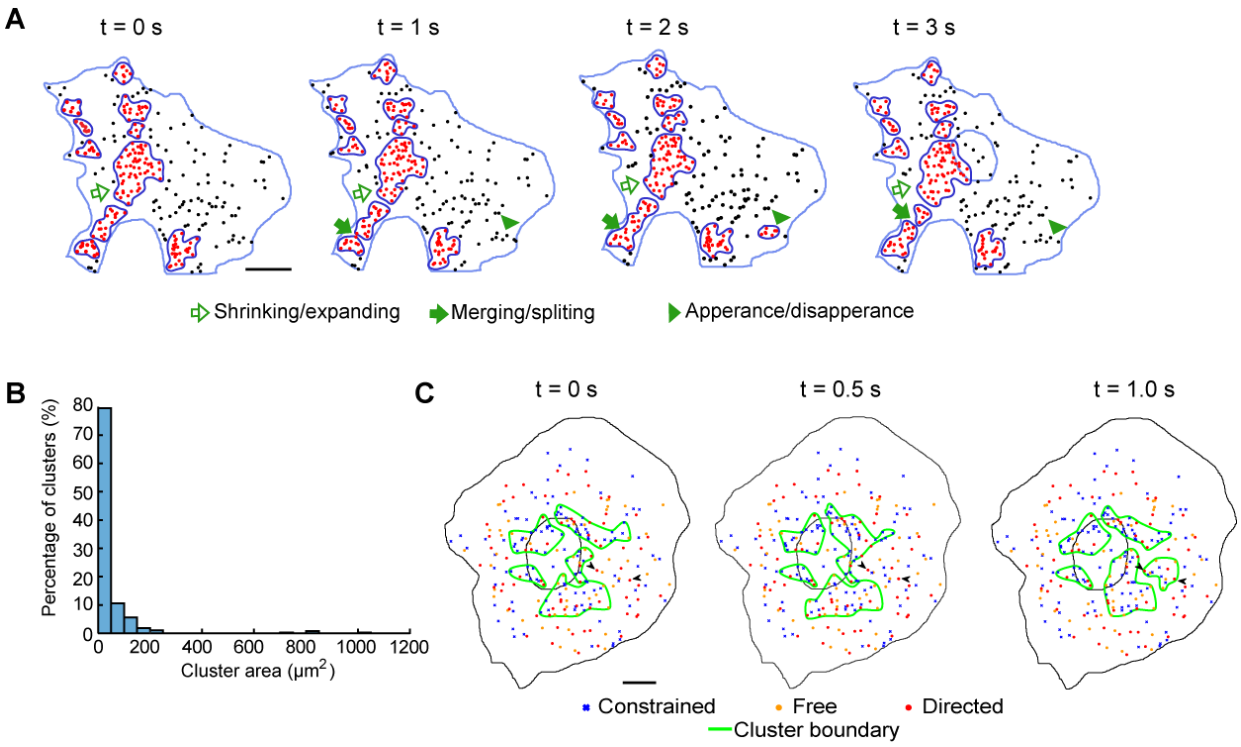

Figure S5. Related to Figure 4. Dynamic turnover and size distribution of lysosomal clusters. (A) Various dynamic turnover events of lysosomal clusters in a COS-7 cell. Scale bar, 15 μm. (B) Size distribution of lysosomal clusters in COS-7 cells. The average area of clusters was 47.2 ± 6.5 μm^2 (mean ± SEM; n = 376 clusters from 9 cells). (C) An example of formation of a cluster, which was mediated by two lysosomes undergoing directed movement (arrowheads) together with lysosomes undergoing constrained diffusion and free diffusion. The entire event was shown in video S4. For simplicity, only large clusters with more than 10 lysosomes were shown. Scale bar, 10 μm.

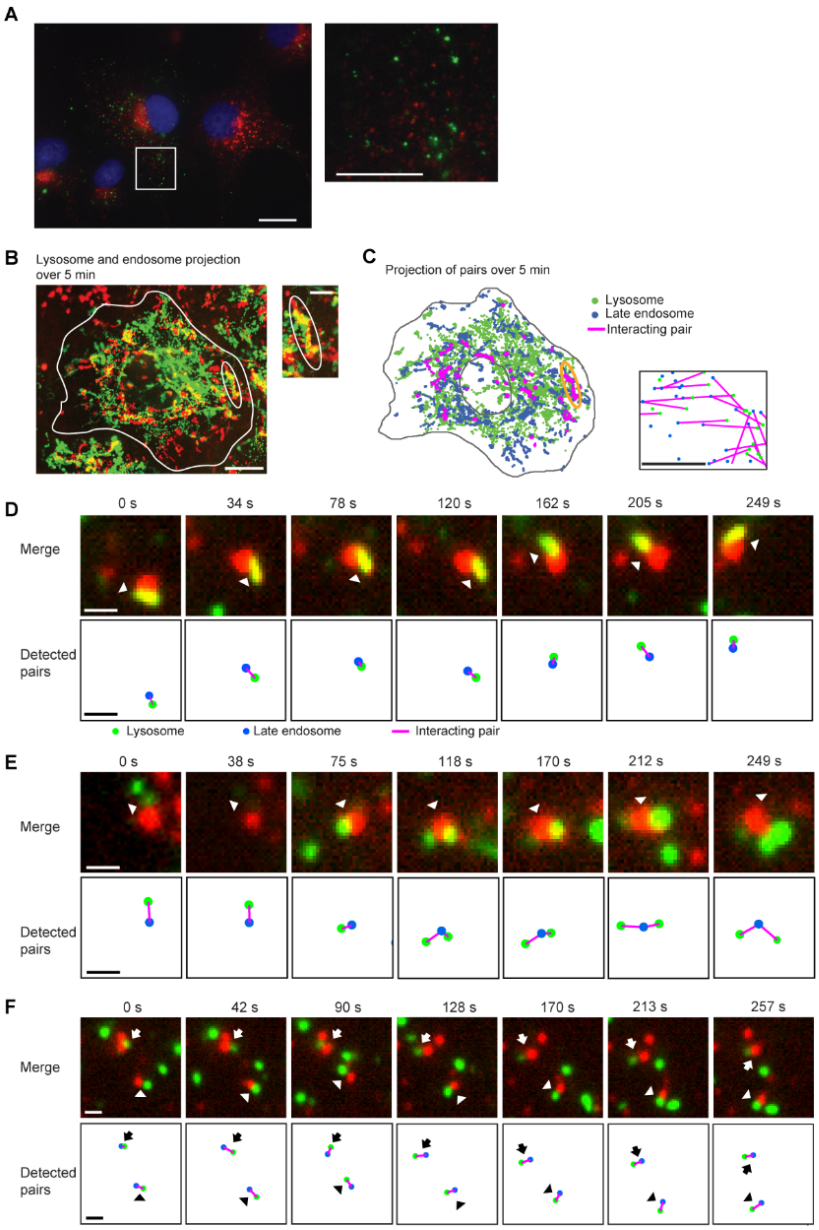

Figure S6. Related to Figure 6 & Figure 7. Fluorescent labeling and computational detection of lysosome-endosome pairs. (A) Validation of specific labeling of lysosomes as terminal endocytic compartments differentiated from late endosomes. Left panel: COS-7 cells labeled with dextran Alexa 488 for lysosome and immunostained for anti-Mannose-6-phosphate receptor (anti-M6PR). Lysosomes are defined as terminal endocytic compartments lacking M6PR (Griffiths et al., 1988; Luzio et al., 2007). They were labeled with a 3 hr pulse of dextran Alexa 488 followed by a 20 hour chase (Bright et al., 2005). Most lysosomes (green) did not colocalize with M6PR (red). Right panel: zoom-in view of the boxed area in the left panel. Blue, cell nucleus. Scale bars: left panel, 20 μm; right panel, 10 μm. (B) Left panel: maximum intensity projection of late endosomes (red) and lysosomes (green) of a 5-minute movie imaged at ~5 seconds per frame. Yellow signals indicate colocalized endosome-lysosome pairs. The circled region shows the trajectory of a computationally detected endosome-lysosome pair. Inset: zoomed in view of the circled region. Scale bars: left panel, 15 μm; inset, 5 μm. (C) Left panel: maximum intensity projection of late endosomes (blue) and lysosomes (green) and detected pairs (magenta), from the same 5-minute movie as in (B). Inset: zoomed-in view of detected pairs. Scale bar: inset, 500 nm. (D-F) Various examples of computationally detected interacting lysosome-endosome pairs (lower rows) and their actual fluorescence signals (upper rows). The pairs of organelles remained associated for at least 4 minutes. (D) An interacting lysosome-endosome pair. (E) An endosome initially interacted with one and then two lysosomes. (F) Two detected lysosome-endosome pairs close to each other. Scale bars: 1 μm.

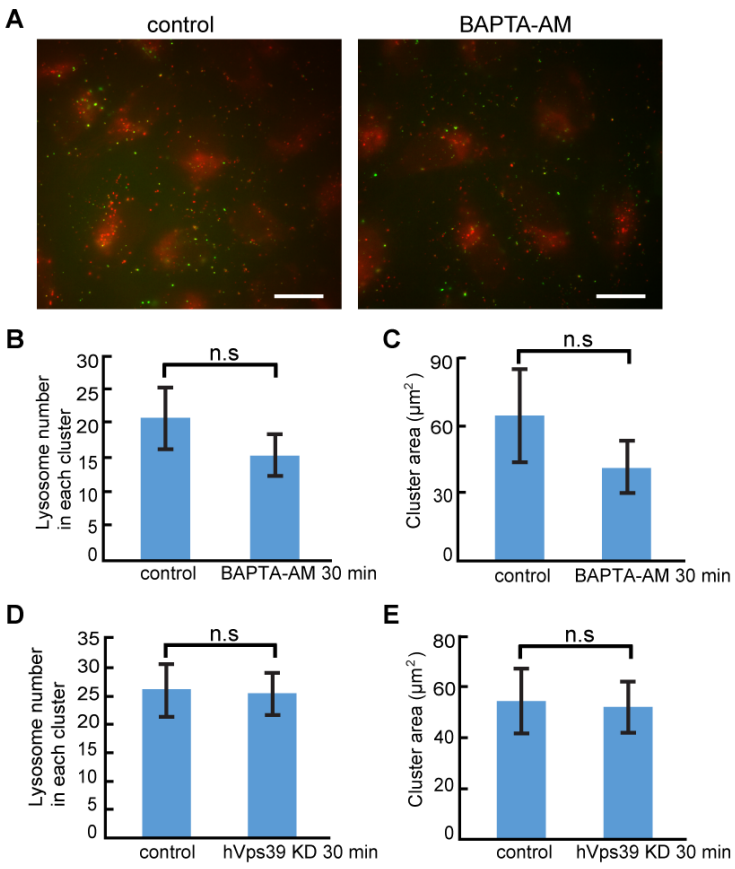

Figure S7. Related to Figure 6 & Figure 7. Clustering of lysosomes does not depend on fusion with late endosomes. (A-B) COS-7 cell labeled with dextran Alexa-488 for 15 min and chased for 30 min for endosomes (green), and co-labeled with Magic Red Cathepsin-B kit for lysosomes (red). (A) Control (DMSO). (B) 10 μM BAPTA-AM treated starting from chasing. Scale bars: 20 μm. (B-E) Error bars show standard deviation. All statistical comparisons were made using one-tailed unpaired student-t tests. (B) Comparison of the number of lysosomes in clusters under control and in BAPTA-AM treated cells (n = 12 cells). p-value: 0.3. (C) Comparison of lysosomal cluster areas under control and in BAPTA-AM treated cells (n = 12 cells). p-value: 0.4. (D) Comparison of the number of lysosomes in clusters under control (n = 12 cells) and in hVps39 knockdown cells (n = 12 cells). p-value: 0.5. (E) Comparison of lysosomal cluster areas under control (n = 12 cells) and in hVps39 knockdown cells (n = 12 cells). p-value: 0.5.

Supplemental Experimental Procedures

Fluorescence Labeling of Organelles

Lysosomes in COS-7 cells were labeled by transfecting 200-300 ng of LAMP1-mCherry. Transfection of COS-7 cells was performed using the Neon electroporation system (Invitrogen, Carlsbad, CA). Briefly, 2×10^5 cells were suspended in a 10 µl pipette tip and electroprated under a pulse voltage of 950 V, a pulse width of 30 ms, and a pulse number of 2. Following transfection, cells were seeded at 6.7×10^4 per 20 mm glass well in 35 mm dishes (MatTek, Ashland, MA) and incubated for 24-48 hours before imaging. Lysosomes in BS-C-1 cells were labeled as described in (Bright et al., 2005; Humphries et al., 2011; Kilpatrick et al., 2015). Briefly, cells were incubated with 0.5 mg/ml dextran Alexa 488, 10000 MW (Molecular Probes, Eugene, OR) for 3-4 hours followed by 16 hours of chasing. Late endosomes and lysosomes in COS-7 cells were co-labelled as described in (Bright et al., 2005; Bright et al., 2015). Briefly, cells were incubated with 0.5 mg/ml dextran Alexa 488 for 3 hours, followed by 20-27 hours of chasing to mark lysosomes. Then cells were incubated with 0.5 mg/ml dextran Alexa 594, 10000 MW (Molecular Probes, Eugene, OR) for 10 minutes followed by 10 minutes of chasing to mark endosomes before imaging. That the co-labeling scheme reliably differentiated late endosomes from lysosomes was validated as described in (Bright et al., 2005; Luzio et al., 2007) by immunostaining of Mannose-6 phosphate receptor (M6PR), a marker present in endosomes but not in lysosomes, using a monoclonal M6PR antibody (MA1-066; Thermo Fisher).

Drug Treatment

To depolymerize microtubules, COS-7 cells were treated with 2.5 µM nocodazole (Sigma-Aldrich, St. Louis, MO) and imaged before and 15 minutes and 30 minutes after treatment for the same cells. To inhibit cytoplasmic dynein, COS-7 cells were treated with 80 µM ciliobrevin D (Sigma-Aldrich, St. Louis, MO) and imaged before and 1 hour after treatment for the same cells. To depolymerize actin filaments, COS-7 cells were treated with 800 nM latrunculin A (Sigma-Aldrich, St. Louis, MO) and imaged before and 7-8 minutes and 15-16 minutes after treatment. To examine the effect of latrunculin A treatment on the actin cytoskeleton, cells were fixed and stained with fluorescent phalloidin (Actin-staining 488 fluorescent phalloidin; Cytoskeleton, Denver, CO) following instructions of the manufacturer. To upregulate lysosomal biogenesis and autophagy, cells were treated with 50 mM trehalose (Sigma-Aldrich, St. Louis, MO) as described in (Palmieri et al., 2017; Porter et al., 2013; Sarkar et al., 2007) and imaged after 12 hours of treatment, or treated with 2µM torin 1 (Tocris Bioscience, Bristol, United Kingdom) as described in (Martina et al., 2012; Thoreen et al., 2009) and imaged after 2 hours up to 14 hours. To verify activation of TFEB by torin-1 treatment (Martina et al., 2012; Thoreen et al., 2009), cells were transfected with TFEB-myc for 24 hours and treated with torin-1 for 4 hours, followed by immunostaining using rabbit anti-myc antibody and mouse anti-rabbit Alexa 594 secondary antibody (ab150128; Abcam, Cambridge, United Kingdom).

Detecting and Tracking Lysosomes in Images

To identify lysosomes in a given image, the Spot Detector plugin of the Icy software (De Chaumont et al., 2012) was used. Cartesian coordinates of detected lysosomes were exported into an Excel XLS file and then imported into our custom MATLAB (MathWorks, Natick, MA) software for further spatial

statistical analysis of their distributions. Lysosomes in images from some experiments, especially these conditions with dense lysosome clusters such as trehalose treatment, were detected using custom implementation of a detector based on the algorithm described in (Ponti et al., 2003), which is included in the MATLAB software. To track movement of lysosomes in a given time-lapse video, the Spot Tracking plugin of Icy (Chenouard et al., 2013; De Chaumont et al., 2012) or TrackMate plugin in ImagJ was used. The recovered lysosome trajectories were exported into an Excel XLS file (SpotTracking) or a CSV file (TrackMate), and then imported into our custom software for further mean-square-displacement (MSD) analysis and spatial statistical analysis. Our software is openly available in source code at https://github.com/ccdlcmu/LysosomeSpatialOrganization_code.

Complete Spatial Randomness Test of Lysosomal Distributions

As an essential step in statistical analysis of spatial point processes (Illian et al., 2008), complete spatial randomness (CSR) test was performed on the distribution of lysosomes at the whole-cell scale to check whether it was entirely random. Specifically, for a given cell, its boundary was manually traced using the *imfreehand* function in MATLAB. The boundary geometry data and the coordinates of detected lysosomes were then passed to *R* for calculation of the Ripley's *K*-function by calling the *spatstat* package. To provide a reference for comparison, a homogeneous Poisson point process was simulated in the same cell geometry with the mean number of simulated lysosomes matching the number of actual lysosomes. The *K*-function was calculated from 99 rounds of simulation. Because the *K*-function for a homogeneous Poisson process has the form $K(r)=\pi r^2$ (Illian et al., 2008), where r denotes neighborhood radius, we subtracted πr^2 from the calculated *K*-functions of both actual and simulated lysosomal distributions for convenience of comparison (Fig. 1C-E). Substantial separation of the actual *K*-function from the reference would indicate non-randomness in distribution.

Characterization of Lysosome Distribution at the Whole-Cell Scale

Lysosome distribution at the whole-cell scale was characterized using statistical distributions of distances between individual lysosomes as well as distances between individual lysosomes and the cell nucleus. These distributions were constructed based on the point process theory of spatial statistical analysis (Diggle, 2014; Illian et al., 2008) and were calculated from detected lysosome positions using our custom software.

(Normalized) Inter-organelle distance distribution: For a given cell, the distribution is calculated from all pairwise distances of its lysosomes (Fig. S1A), which characterizes spacing between lysosomes at the whole-cell scale. Specifically, for the i^{th} and j^{th} lysosomes, whose positions are denoted $\left(p_x^i, p_y^i\right)$ and $\left(p_x^j, p_y^j\right)$, respectively, their inter-organelle distance $D_{IO}(i,j)$ is their Euclidean distance, $D_{IO}(i,j) \triangleq \sqrt{\left(p_x^i - p_x^j\right)^2 + \left(p_y^i - p_y^j\right)^2}$, $i \neq j$, $i,j \in [1..N]$, where N is the total number of lysosomes. To account for variations in cell sizes, the normalized inter-organelle distance $\tilde{D}_{IO}(i,j) \triangleq D_{IO}(i,j) / D_{IO}^{Max}$ is used, where $D_{IO}^{Max} \triangleq \max\{D_{IO}(i,j)\}$ is the maximum inter-organelle distance. For each cell, after calculating its complete set of normalized inter-organelle distances, $\left\{\tilde{D}_{IO}(i,j),\ i \neq j,\ i,j \in [1..N]\right\}$, the

probability density function (pdf) of the distances is estimated using MATLAB function *ksdensity* with default parameters, including a normal kernel whose bandwidth is optimized for density estimation.

(Normalized)To-nucleus distance distribution: For analysis given cell, the boundary of its nucleus (from DAPI-staining or DIC image) is manually traced and then approximated by the set of boundary points using the MATLAB function *imfreehand*. We denote the set of boundary points as $S(C)$. For the i^{th} lysosome, its to-nucleus distance $D_{TN}(i)$ is its distance to the nearest nucleus boundary point, defined as $D_{TN}(i) \triangleq \min_{(s_x^A, s_y^A) \in S(A)} \sqrt{\left(p_x^i - s_x^A\right)^2 + \left(p_y^i - s_y^A\right)^2}$. The normalized to-nucleus distance $\tilde{D}_{TN}(i) \triangleq D_{TN}(i) / D_{TN}^{Max}$ is used to account for variations in cell sizes, where $D_{TN}^{Max} \triangleq \max\{D_{TN}(i)\}$ is the maximum to-nucleus distance. For each cell, the probability density function of its complete set of normalized to-nucleus distances, $\left\{\tilde{D}_{TN}(i)\right\}$, $i \in [1..N]$, is estimated using MATLAB function *ksdensity* with the same parameter setting as for the inter-organelle distance distribution.

Nearest-neighbor distance distribution: For a given cell, this distribution is calculated from all nearest neighbor distances of its lysosomes. It characterizes the shortest distances between individual lysosomes at the whole-cell level. Specifically, for the i^{th} lysosome, its nearest-neighbor distance $D_{NN}(i)$ is defined as $D_{NN}(i) \triangleq \min\left\{D_{IO}(i,j),\ i \neq j,\ j \in [1..N]\right\}$. The probability density function of the complete set of nearest-neighbor distances, $\left\{D_{NN}(i),\ i \in [1..N]\right\}$ is estimated using MATLAB function *ksdensity* with the same parameter setting as for the inter-organelle distance distribution.

Quantification of Differences in Lysosome Distributions at the Whole-Cell Scale

After defining the distance distributions for characterizing lysosome spatial distributions at the whole-cell level, it is often necessary to compare such distributions at two different time points in the same cell or between two different cells. To compare two distance distributions, represented by pdf_i and pdf_j, respectively, we quantified their difference using the following intersection measure (Cha, 2007), also referred to as the Sorensen distance, which quantifies the level of non-overlap between the two distributions.

$$D_{INT}\left(pdf_i, pdf_j\right) \triangleq \frac{\int_0^L \left|pdf_i(x) - pdf_j(x)\right| dx}{\int_0^L pdf_i(x)\,dx + \int_0^L pdf_j(x)\,dx} = \frac{1}{2}\int_0^L \left|pdf_i(x) - pdf_j(x)\right| dx$$

For normalized distance distributions, L equals 1. For non-normalized distance distributions, L equals the larger one of the two maximal distances of the two distributions.

Classification of Lysosomes Based on their Modes of Movement

Trajectories of lysosomes were recovered through single particle tracking as described above. From each trajectory that lasts at least 25 frames, which correspond to 2.4 seconds in imaging, the mean square displacement (*MSD*) function was calculated as described in (Saxton, 1997) with the maximum lag of 24 frames. Because *MSD* is a function of time, we assume the following simplified model:

$$MSD(\tau) = A\tau^{\alpha} + B$$

in which α can be used to classify different modes of movement (Qian et al., 1991). To determine α, the *MSD* was fitted using the MATLAB function *nlnfit*. The mode of movement of the corresponding lysosome was then classified according to the following table:

α	**Mode of Movement**
α<0.9	Constrained diffusion
0.9≤ α≤1.2	Free diffusion
α>1.2	Directed movement

Density-Based Clustering of Lysosomes

To study collective behavior of lysosomes, clusters of lysosomes were identified using a density based clustering algorithm DBSCAN (Ester et al., 1996). Briefly, a lysosome was randomly selected as a seed. The algorithm then searched a circular neighborhood of radius *r* centered at the seed. If the total number of lysosomes in the neighborhood was less than a preset threshold *k*, the seed was excluded as a noise point. If the number equaled or exceeded the threshold *k*, the seed lysosome with its neighbors were considered to be in a high density region and incorporated in a cluster. The incorporated neighboring lysosomes were then set as new seeds. This process was repeated until the number of lysosomes in a new neighborhood fell below threshold *k*. The algorithm repeated this process for the rest of lysosomes not in any cluster. Note that in this way, each cluster has at least *k* lysosomes within a neighborhood of radius *r*. A threshold setting of $k \geq 4$ was recommended for good performance and reasonable computational cost (Ester et al., 1996). We chose a threshold of $k = 5$ to balance stringency of thresholding and sensitivity for identifying small clusters.

To set the neighborhood radius *r* for a given threshold *k*, the spatial densities of lysosomes should be higher than the spatial densities of a random and uniform distribution of lysosomes with the same total number of lysosomes. This distribution was determined through computer simulation. Specifically, for a given cell, 99 simulations were performed using the *spatstat* package function *runifpoint*, which used the rejection method (Illian et al., 2008) to generate a random and uniform point pattern inside the cell geometry, with the number of simulated lysosomes matching the actual number of lysosomes in the cell. The spatial density distribution of the simulated point pattern was then computed using the *spatstat* function *density.ppp*. A threshold spatial density, denoted λ_{thresh} was then set to be 95% of the maximal spatial density from simulation. The search radius was then calculated as $r = \sqrt{k / \pi\lambda_{thresh}}$, with a threshold of $k = 5$. For a time-lapse movie, the simulation was performed based on the number of lysosomes in the first frame. The search radius determined was then used for the rest of the frames.

Controlling Cell Shape Using Patterned Protein Substrates

Cells were grown into defined shapes by culturing them on patterned protein substrates made by micro-contact printing (Azioune et al., 2009; Singhvi et al., 1994; Xia and Whitesides, 1998).

PDMS stamp fabrication: Protein substrate patterns were designed using AutoCAD (Autodesk, San Rafael, CA). A plastic mask with designed circular substrate patterns (68 μm in diameter) was produced by

CAD/ART Services (Bandon, OR) at 10-μm resolution. Master molds were fabricated by spin coating a 4-μm thick layer of SPR 220-3.0 (MicroChem, MA) onto a 2 μm thick coverslip glass (Fisher Scientific, Hampton, NH) followed by UV exposure at 365 nm using a custom made UV illumination system. Polydimethylsiloxane (PDMS) stamps were made by mixing Sylgard 184 (Dow Corning, MI, US) PDMS base with curing agent at the ratio of 1:10, followed by 1 hour defoaming under vacuum and curing for 12-24 hours at 65 °C. Stamps approximately 1 cm × 1 cm in size were cut from the PDMS blocks for micro contact printing (Azioune et al., 2009).

Micro-contact printing of protein substrates: PDMS stamps were sonicated in 75% ethanol for 30 minutes and dried by nitrogen blowing under a laminar hood. The stamps were then coated with 200 μL of 20 μg/ml fibronectin (Thermo Fisher Scientific, Waltham, MA) in PBS and incubated at room temperature for 1 hour. Alexa 594 conjugated fibrinogen (Molecular Probes, Eugene, OR) was added to the fibronectin solution at a final concentration of 8 μg/ml for visualization of printed patterns (Azioune et al., 2009). The stamps were rinsed in deionized water and dried under a laminar hood. The stamps were then placed with the pattern side down on glass surfaces in 35 mm MatTek dishes (Ashland, MA) with 2.0 cm wells. After 1 hour the stamps were removed to release patterned proteins (Palchesko et al., 2012). To prevent cell attachment in unpatterned area, the printed glass surfaces were coated with 0.1 mg/ml of PLL-g-PEG (Surface Solutions, Dübendorf, Switzerland) in PBS for 1 hour and rinsed with PBS for three times.

Cell culture on patterned protein substrates: Dextran-488 labeled BS-C-1 cells were trypsinized 16 hours after labeling and seeded onto patterned substrates. Unattached cells were removed 45-60 min after seeding. Imaging was performed 4-7 hours after seeding.

Testing Whether Distinct Lysosomal Spatial Distributions in Single Cells are a Secondary Effect of Distinct Cell Shapes

To compare the spatial distributions of lysosomes in different cells, we selected the first frame from the time-lapse movie of each cell and compared the three lysosomal distance distributions among all cells in a pairwise fashion (Fig. S2A-C; blue lines) because the distribution within each cell remained stable over time. We found that the three distributions differed significantly in all or most of the pairwise comparisons (Fig. S2D, “unpatterned” columns), indicating that lysosomes maintain distinct spatial distributions in single cells.

To investigate what causes the variations among single cells in their lysosomal distributions, we examined two sources. First, temporal variations of the three distance distributions within single cells, which we refer to as *intracellular* variations, surely contribute to the variations among different cells, which we refer to as *intercellular* variations. Overall, however, we found that the contribution was very small because the average level of intracellular variations was significantly lower than the average level of intercellular variations (Fig. S2E). Second, different cells often exhibit distinct shapes (Fig. S2F). To check whether variations among different cells in their lysosomal distributions are merely a secondary effect of differences in their shapes, we grew cells into approximately the same size and circular shape on patterned protein substrates (Fig. S2G-H; Video S2). We then checked the intercellular variations of the three distance distributions among the patterned cells (Fig. S2A-C; green lines). All or most of the pairwise comparisons of these distributions showed significant differences (Fig. S2D, “patterned” columns). For the normalized inter-organelle distance distribution and the normalized to-nucleus distance distribution, the levels of

intercellular variations among patterned cells remained substantial, though significantly lower than among unpatterned cells (Fig. S2I). For the nearest-neighbor distance distribution, there was no significant difference between unpatterned and patterned cells in terms of intercellular variations (Fig. S2I). Taken together, these results show that, although differences in cell shapes contribute to intercellular variations in spatial distributions of lysosomes, such variations in unpatterned cells are not merely a secondary effect of the distinct cell shapes but, instead, are mediated by intrinsic intracellular mechanisms. This further indicates that lysosomes are spatially organized.

Estimating Spatial Density Distributions of Lysosomes

The spatial density distribution of lysosomes within a single cell represent the number of lysosomes per unit area at different locations inside that cell. This distribution was estimated using the *R* package *spatstat* (Baddeley et al., 2016; Baddeley and Turner, 2005). Specifically, for a given cell, with its size measured in micrometers and its shape represented by a polygon, a window of the same size and shape was created using the *R* function *owin*, Lysosomes detected within the cell as described above were used to create a point pattern object using the *R* function *ppp*. The spatial density distribution was then estimated using a kernel-based method by calling the *R* function *density.ppp.* The estimated spatial density distribution $\hat{\lambda}_\sigma(x)$ is defined by the following equation:

$$\hat{\lambda}_\sigma(x) = \frac{1}{N}\sum_{i=1}^{N} K_\sigma(x - x_i), \quad x, x_i \in R^2,$$

where $K_\sigma(\cdot)$ is an isotropic 2D Gaussian kernel whose standard deviation σ is also referred to as the bandwidth of estimation, x represents any given position within the cell, x_i is the position of the i^{th} lysosome, and N is the total number of lysosomes in the cell. The grid size for estimating the spatial density distribution was set to be 1 μm. The grid number was determined by the size of the smallest rectangle that circumscribes the cell. No edge correction was performed. Note that the density distribution estimated by *spatstat* is not in the form of a probability density function. Instead, it directly represents the number of lysosomes per unit area and is thus convenient for interpretation.

The estimation bandwidth σ was chosen using the R function *bw.diggle* by minimizing the means squared error of the density estimation (Berman and Diggle, 1989). For estimating spatial density distributions of lysosomes over time in a time-lapse movie, σ was chosen based on the first frame and then kept the same for all subsequent frames.

Immunofluorescence

Cells were grown in 35mm dishes (MatTek, Ashland, MA) and fixed with 4 % formaldehyde for 8 minutes and permeablized in 0.2% Triton X-100/PBS for 5 minutes at room temperature. Cells were then blocked with 5% normal goat serum for 1 hour and incubated with primary antibodies at 4°C overnight and secondary antibodies at room temperature for 1 hour. After each antibody incubation step, cells were washed five times with DPBS with Ca^{2+} and Mg^{2+}, 5 minute each time. Nuclei were then labeled with Hoechst 33342 (Sigma-Aldrich). Samples were imaged in DPBS with Ca^{2+} and Mg^{2+}. To differentiate lysosomes from late endosomes, mouse monoclonal antibody against mannose 6-phosphate receptor

(1:500, Thermo Fisher MA1-066) was used. The secondary antibody used was Alexa Fluor 594-conjugated goat anti-rabbit IgG (1:400, Abcam ab150116, Cambridge, UK).

Calculating ER Spatial Density within Lysosomal Clusters

To study the spatial relations between lysosomal clusters and the ER network, we calculated the local spatial density of the ER network within the clusters. Specifically, ER spatial densities in lysosome cluster regions and non-cluster regions of the same shapes were compared. Here, density is defined by the percentage of pixels occupied by ER inside a region of interest (ROI), $\lambda_{ER} = \frac{N_{pixels\ in\ ROI}}{N_{pixels\ total}} \times 100\ \%$, where $N_{pixels\ in\ ROI}$ denotes the number of pixels belonging to the ER network in a selected region, and $N_{pixels\ total}$ denotes the total number of pixels in the selected region. Clustering of lysosomes were performed with DBSCAN as described above. Cluster boundaries were then detected using MATLAB function *boundary*.

Segmentation of ER: Wide-field fluorescent images of ER were first deconvolved using the software Autoquant (Bitplane, Belfast) to reduce blurring. The deconvolved images were then segmented with a local adaptive thresholding method using MATLAB function *imbinarize* with an input option of 'adaptive'.

Detection of ER densities in lysosome clusters: To obtain ER densities in clustering regions, clustering of lysosomes was performed with the DBSCAN method. Cluster boundaries were then determined using the MATLAB function *boundary*, and the regions within the boundaries were examined in the corresponding ER segmentation results. The pixels with ER signals within a boundary were counted and divided by the total number of pixels within this boundary to obtain the ER density λ_{ER}. To obtain ER densities in non-cluster regions, the cluster boundaries were moved to non-cluster regions, and the ER densities in this non-cluster boundary were then calculated. For each selected cluster boundary, 3-5 non-cluster regions were randomly chosen so that most of the non-cluster regions in a cell were covered. However, this analysis was performed only in regions in which the ER network could be properly segmented.

Analyzing Interactions between Lysosomes and Endosomes

Nearest-neighbor distribution between lysosomes and endosomes: The nearest neighbor distance distribution between lysosomes was extended to characterize the relative positioning of lysosomes with late endosomes. For each lysosome, its distance to the nearest endosome was calculated. Then the probability density function was estimated from the nearest neighbor distance of all lysosomes using MATLAB function *ksdensity* and was referred to as the nearest-neighbor distance distribution between lysosomes and the partner organelles.

Detecting interacting pairs of organelles: Candidates of interacting pairs were detected first based on spatial proximity. A pair of organelle was considered as a candidate if their distance was smaller than a threshold distance $D_{\min}$, which was determined based the following formula

$$D_{\min} = D_{drift} + \max\left(D_{nn}, D_{org}\right).$$

This threshold was calculated for each cell and typically ranged from 0.4 μm to 0.8 μm. D_{drift} denotes the distances organelles travel within the lag of switching between channels during imaging. For the imaging setup of this study, the lag is roughly 1 s, and the corresponding drift was estimated to be ~0.2 μm based on single particle tracking of late endosomes and lysosomes. The nearest neighbor distance D_{nn} was chosen as the lower 10% quantile of the nearest neighbor distance between lysosomes and the partner organelles. Lastly, the diameters of organelles were also considered when D_{nn} is smaller than the lower bound of organelle size D_{org}, which can occur because the position of an organelle was represented by its centroid. The lower bound of organelle size D_{org} was set to be 0.25 μm for COS-7 cells and 0.4 μm for U2OS cells, given the diffraction limit of light microscopy and the fact that late endosomes and lysosomes are often larger than this size.

From the candidate pairs, interacting pairs were identified if the time they stay within the distance threshold is longer than a time threshold. This threshold is set to be 25 seconds based on a >85% quantile of the time different pairs of organelles staying with the distance threshold. The detection results were then visually inspected to exclude errors. Under the distance threshold and the time threshold selected, more than 80% of the detected interacting pairs of lysosomes and endosomes had a spatial overlap of their fluorescence signal during at least 80% of the time they stayed within the threshold distance to each other.

Detecting interacting pairs within organelle clusters: To detect interacting pairs inside organelle clusters, the MATLAB function *boundary* was used to determine boundaries of identified organelle clusters, represented as polygons. Then the function *inpolygon* was used to select interacting pairs. To detect interacting pairs inside overlaying regions of clusters of both types of organelles, endosomes in any interacting pair that lied within or on boundary of any lysosome cluster $C_{lyso}^{(j)},\ j = 1,2,\dots m,$ were detected as candidates. Then the candidate endosomes that fell within or on the boundaries of any endosome cluster(s) were selected. After this step, we accepted the candidate pair if the interacting lysosomes also reside in the same endosome cluster boundary and the lysosome cluster boundary.

Disruption of Lysosome-Endosome Fusion

Knockdown of the HOPS complex in U2OS cells was performed using the on-target Smartpool human Vps39 siRNAs (#9: gcacaaaagaaacgguuca, #10: gcacgacgcuuucgagcca, #11: gugaggagguguuacggau and #12: ggaauacagugcuaguuga) (Dharmacon) by transfecting the cells using the Neon electroporation system. Non-targeting control pool siRNAs (D-001810-10-05, Dharmacon) were used as control. Briefly, around 2×10^5 cells were suspended in a 10 μl pipette tip and electroporated under a pulse voltage of 1230 V, a pulse width of 10 ms, and a pulse number of 4. Following transfection, cells were seeded at 5-6.7$\times10^4$ per 20 mm glass well in 35 mm dishes and incubated for 3 days before imaging. Knockdown of hVps39 mRNA was verified by RT-PCR. mRNA was isolated from cells using TRIzol (Invitrogen) according to the manufacturer's instructions, and converted to cDNA using 2 μg of RNA with the GeneAmp RNA PCR system (Applied Biosystems, Carlsbad, CA). RT-PCR was performed using the T7300 Real Time System (Applied Biosystems, Carlsbad, CA) with 2× SYBR Green (Fermentas, Glen Burnie, MD) and primers (Forward: GAGCCAAAAGCCAACCTCCA; reverse: GCAGAAGGTTGAGGGCCTTG) ordered from Integrated DNA Technologies (Coralville, IA) . cDNA dilutions of 1:15 were used for final qPCR reactions,

and 10 µl reactions were run in triplicate on the following parameters: 2 minutes at 50°C, 10 minutes at 95 °C, and 40 cycles at 95 °C for 15 seconds followed by 60 °C for 1 minute.

To determine the disruption of endosome-lysosome fusion, the cells were first incubated with 1.25 mg/ml dextran Alexa 488 for 15 min, and then washed with culture media, followed by lysosome labeling using Magic Red Cathepsin-B (ImmunoChemistry Technologies, Bloomington, MN) at a dilution ratio of 1:1300 (10 times lower than the manufacturer's instructions) for 10 min. Cells were imaged 30 min after washout of the dextran dye. For acute disruption of lysosome-endosome fusion, labeling and BAPTA-AM treatment of U2OS were performed largely according to (Colletti et al., 2012). Briefly, cells were first incubated with 1.5 mg/ml dextran Alexa 488 for 15 min to label late endosomes, and then washed with culture media and treated with 10 µM BAPTA-AM (Merck Millipore, Burlington, MA), followed by lysosome labeling using Magic Red Cathepsin-B. Cells were imaged after 30 min of treatment.

Supplemental References

Azioune, A., M. Storch, M. Bornens, M. Théry, and M. Piel. 2009. Simple and rapid process for single cell micro-patterning. *Lab Chip*. 9:1640-1642.

Baddeley, A., E. Rubak, and R. Turner. 2016. Spatial Point Patterns: Methodology and Applications with R. Chapman & Hall/CRC.

Baddeley, A., and R. Turner. 2005. spatstat: An R package for analyzing spatial point patterns. *J. Stat. Softw.* 12:1-42.

Berman, M., and P. Diggle. 1989. Estimating weightedintegrals of the second-order Intensity of a spatial point process. *J. R. Stat. Soc. Series B Stat. Methodol.* 51:81-92.

Bright, N.A., M.J. Gratian, and J.P. Luzio. 2005. Endocytic delivery to lysosomes mediated by concurrent fusion and kissing events in living cells. *Curr. Biol.* 15:360-365.

Bright, N.A., L. Wartosch, and J.P. Luzio. 2015. Lysosome fusion in cultured mammalian cells. *Methods Cell Biol.* 126:101-118.

Cha, S.-H. 2007. Comprehensive survey on distance/similarity measures between probability density functions. *International Journal of Mathematical Models and Methods in Applied Sciences*. 1:300-307.

Chenouard, N., I. Bloch, and J.C. Olivo-Marin. 2013. Multiple hypothesis tracking for cluttered biological image sequences. *IEEE Trans. Pattern Anal. Mach. Intell.* 35:2736-3750.

De Chaumont, F., S. Dallongeville, N. Chenouard, N. Herve, S. Pop, T. Provoost, V. Meas-Yedid, P. Pankajakshan, T. Lecomte, Y. Le Montagner, T. Lagache, A. Dufour, and J.-C. Olivo-Marin. 2012. Icy: an open bioimage informatics platform for extended reproducible research. *Nat. Meth.* 9:690-696.

Diggle, P.J. 2014. Statistical Analysis of Spatial and Spatiotemporal Point Patterns. CRC Press.

Ester, M., H.-P. Kriegel, #246, r. Sander, and X. Xu. 1996. A density-based algorithm for discovering clusters a density-based algorithm for discovering clusters in large spatial databases with noise. *In* Proceedings of the Second International Conference on Knowledge Discovery and Data Mining. AAAI Press, Portland, Oregon. 226-231.

Griffiths, G., B. Hoflack, K. Simons, I. Mellman, and S. Kornfeld. 1988. The mannose 6-phosphate receptor and the biogenesis of lysosomes. *Cell*. 52:329-341.

Humphries, W.H.t., C.J. Szymanski, and C.K. Payne. 2011. Endo-lysosomal vesicles positive for Rab7 and LAMP1 are terminal vesicles for the transport of dextran. *PLoS One*. 6:e26626.

Illian, J., A. Penttinen, H. Stoyan, and D. Stoyan. 2008. Statistical Analysis and Modeling of Spatial Point Patterns. Wiley.

Kilpatrick, B.S., E.R. Eden, L.N. Hockey, C.E. Futter, and S. Patel. 2015. Chapter 1 - Methods for monitoring lysosomal morphology. *In* Methods Cell Biol. Vol. 126. P. Frances and P. Nick, editors. Academic Press. 1-19.

Luzio, J.P., P.R. Pryor, and N.A. Bright. 2007. Lysosomes: fusion and function. *Nat. Rev. Mol. Cell Biol.* 8:622-632.

Martina, J.A., Y. Chen, M. Gucek, and R. Puertollano. 2012. MTORC1 functions as a transcriptional regulator of autophagy by preventing nuclear transport of TFEB. *Autophagy*. 8:903-914.

Palchesko, R.N., L. Zhang, Y. Sun, and A.W. Feinberg. 2012. Development of polydimethylsiloxane substrates with tunable elastic modulus to study cell mechanobiology in muscle and nerve. *PloS one*. 7:e51499.

Palmieri, M., R. Pal, H.R. Nelvagal, P. Lotfi, G.R. Stinnett, M.L. Seymour, A. Chaudhury, L. Bajaj, V.V. Bondar, and L. Bremner. 2017. mTORC1-independent TFEB activation via Akt inhibition promotes cellular clearance in neurodegenerative storage diseases. *Nat. Commun.* 8:14338.

Ponti, A., P. Vallotton, W. Salmon, C. Waterman-Storer, and G. Danuser. 2003. Computational analysis of F-actin turnover in cortical actin meshworks using fluorescent speckle microscopy. *Biophys. J.* 84:3336-3352.

Porter, K., J. Nallathambi, Y. Lin, and P.B. Liton. 2013. Lysosomal basification and decreased autophagic flux in oxidatively stressed trabecular meshwork cells: implications for glaucoma pathogenesis. *Autophagy*. 9:581-594.

Qian, H., M.P. Sheetz, and E.L. Elson. 1991. Single particle tracking. Analysis of diffusion and flow in two-dimensional systems. *Biophys J*. 60:910-921.

Sarkar, S., J.E. Davies, Z. Huang, A. Tunnacliffe, and D.C. Rubinsztein. 2007. Trehalose, a novel mTOR-independent autophagy enhancer, accelerates the clearance of mutant huntingtin and α-synuclein. *J. Biol. Chem.* 282:5641-5652.

Saxton, M.J. 1997. Single-particle tracking: the distribution of diffusion coefficients. *Biophy J*. 72:1744-1753.

Singhvi, R., A. Kumar, G.P. Lopez, G.N. Stephanopoulos, D.I. Wang, G.M. Whitesides, and D.E. Ingber. 1994. Engineering cell shape and function. *Science*. 264:696-699.

Thoreen, C.C., S.A. Kang, J.W. Chang, Q. Liu, J. Zhang, Y. Gao, L.J. Reichling, T. Sim, D.M. Sabatini, and N.S. Gray. 2009. An ATP-competitive mammalian target of rapamycin inhibitor reveals rapamycin-resistant functions of mTORC1. *J. Biol. Chem.* 284:8023-8032.

Xia, Y., and G.M. Whitesides. 1998. Soft lithography. *Annu. Rev. Mater. Sci.* 28:153-184.